

Article

Structures, Bonding and Sensor Properties of Some Alkaline *o*-Phthalatocuprates

Sergey V. Gladnev, Mikhail V. Grigoryev, Mariya A. Kryukova, Evgenia M. Khairullina, Ilya I. Tumkin ,
Nikita A. Bogachev, Andrey S. Mereshchenko  and Mikhail Y. Skripkin * 

Institute of Chemistry, Saint-Petersburg State University, 7/9 Universitetskaya Emb.,
199034 St. Petersburg, Russia; st069020@student.spbu.ru (S.V.G.); mikegrig@inbox.ru (M.V.G.);
m.a.kryukova@spbu.ru (M.A.K.); e.khairullina@spbu.ru (E.M.K.); i.i.tumkin@spbu.ru (I.I.T.);
n.a.bogachev@spbu.ru (N.A.B.); a.mereshchenko@spbu.ru (A.S.M.)

* Correspondence: m.skripkin@spbu.ru; Tel.: +7-906-246-96-32

Abstract: Comprehensive study of the structure and bonding of disodium, dipotassium and diammonium di-*o*-phthalatocuprates(II) dihydrates has been undertaken. The crystal structure of ammonium *o*-phthalatocuprate has been determined. The identity of structures of phthalatocuprate chains in potassium and ammonium salts has been revealed. Vibrational spectra of all three compounds have been recorded, and the assignment of vibrational bands has been made. Force field calculations have shown a minor effect of outer-sphere cations (Na^+ , K^+ , NH_4^+) on both intraligand (C-O) and metal–ligand bond strengths. Synthesized compounds have been tested as electrochemical sensors on D-glucose, dopamine and paracetamol. Their sensitivity to analytes varied in the order of $\text{Na}^+ > \text{K}^+ > \text{NH}_4^+$. This effect has been explained by the more pronounced steric hindrance of copper ions in potassium and ammonium salts.

Keywords: alkaline *o*-phthalatocuprates; crystal structure; vibrational spectra; force constants; electrochemical sensors; D-glucose; paracetamol; dopamine



Citation: Gladnev, S.V.; Grigoryev, M.V.; Kryukova, M.A.; Khairullina, E.M.; Tumkin, I.I.; Bogachev, N.A.; Mereshchenko, A.S.; Skripkin, M.Y. Structures, Bonding and Sensor Properties of Some Alkaline *o*-Phthalatocuprates. *Materials* **2021**, *14*, 5548. <https://doi.org/10.3390/ma14195548>

Academic Editor: Lucia Carlucci

Received: 28 July 2021

Accepted: 17 September 2021

Published: 24 September 2021

Publisher's Note: MDPI stays neutral with regard to jurisdictional claims in published maps and institutional affiliations.



Copyright: © 2021 by the authors. Licensee MDPI, Basel, Switzerland. This article is an open access article distributed under the terms and conditions of the Creative Commons Attribution (CC BY) license (<https://creativecommons.org/licenses/by/4.0/>).

1. Introduction

Copper-based metal–organic frameworks (MOFs) with polycarboxylate linkers have recently attracted attention in the field of electrochemical sensors for the detection of different analytes [1–4] due to their potential for increasing electrode/electrolyte interfaces and reducing mass consumption by tuning single atomic metal centers. For example, Cu(BTC) MOF (BTC: trimesic acid) has shown peroxidase-like activity for electrochemical detection of H_2O_2 [5] and catechol [6], respectively. Cu-based MOFs, consisting of Cu^{2+} ions and ligands such as TPA (TPA: terephthalic acid) and BTC, have shown good electrochemical properties and excellent catalytic performance in electrochemical sensors for the detection of analytes such as glucose, H_2O_2 , etc. [7,8]. Though numerous studies have been conducted in this field, there are mostly only empirical observations of electrocatalytic activity towards target analytes [9,10], and the factors affecting the sensor properties of the different types of materials with similar structures have not yet been fully identified. In this regard, in this work the effect of an outer-sphere cation (Na^+ , K^+ , NH_4^+) on structure and bonding in alkaline di-*o*-phthalatocuprate dihydrates was studied in detail to reveal the major factors that determine sensor activity of phthalatocuprates towards D-glucose.

2. Materials and Methods

2.1. Reagents

Copper(II) Carbonate Basic (>95%), Potassium Hydrogen Phthalate (>99.95%), Phthalic Acid (>98%), Sodium Hydroxide (>99.5%), D-Glucose, Paracetamol, Dopamine Hydrochloride (all—European Pharmacopoeia (EP) Reference Standard), PBS buffer, Nafion

(5 wt% solution) and Ammonia (32% aqueous solution) were purchased from Sigma-Aldrich Ltd. (Darmstadt, Germany), Sodium Hydrogen Phthalate (> 99%) was supplied by Advanced Technology & Industrial Co., Ltd. (Hong Kong, China). All the reagents were used without further purification.

2.2. Synthesis of Alkaline di-*o*-Phthalatocuprates(II) Dihydrates

Disodium(I) and dipotassium(II) di-*o*-phthalatocuprates(II) dihydrates have been synthesized according to the method described in [11]. Copper(II) carbonate basic was dissolved in an aqueous solution containing a stoichiometric amount of alkaline hydrogen phthalate. As no ammonium hydrogen phthalate was available, this was prepared in situ simply by mixing equimolar amounts of ammonia and phthalic acid, and then stoichiometric amount of copper carbonate basic was added under stirring to obtain diammonium(III) di-*o*-phthalatocuprate(II) dihydrate. The solutions were allowed to stay at room temperature for slow evaporation; as a result, blue elongated prismatic crystals suitable for X-ray analysis were obtained for all three samples.

2.3. XRD Characterization

X-ray powder diffraction (XRD) measurements were performed on a D2 Phaser (Bruker, Billerica, MA, USA) X-ray diffractometer using Cu K α radiation ($\lambda = 1.54056 \text{ \AA}$). Experimental powder diffractograms are compared with calculated ones at Figure 1. As no crystallographic data for III are available so far, single-crystal X-ray diffraction analysis was undertaken. Data were collected using Agilent Technologies «Xcalibur» diffractometer K using a monochromatic radiation source (MoK α radiation, $\lambda = 0.71073$). The structure was solved using the ShelXT [12] structure solution program by Intrinsic Phasing and refined with the ShelXL [12] incorporated in the Olex2 refinement package [13]. Empirical absorption correction was applied in the CrysAlisPro (Agilent Technologies, Santa Clara, CA, USA, 2014) program complex using spherical harmonics, implemented in SCALE3 ABSPACK scaling algorithm. The carbon-bound H atoms were placed in calculated positions and were included in the riding model approximation, with $U_{iso}(\text{H})$ set to $1.2U_{eq}(\text{C})$ and C–H 0.93 \AA for the CH groups, $U_{iso}(\text{H})$ set to $1.6U_{eq}(\text{N})$ and N–H in the corresponding bond lengths for the NH groups, and $U_{iso}(\text{H})$ set to $1.5U_{eq}(\text{O})$ and O–H 0.85 \AA for the OH groups. The crystallographic parameters and the structure refinement statistics for III at $T = 293(2) \text{ K}$ are as follows: $\text{C}_{16}\text{H}_{20}\text{CuN}_2\text{O}_{10}$, $M_w = 463.88 \text{ g/mol}$, space group $I2/a$, $a = 7.9889(3) \text{ \AA}$, $b = 21.2012(8) \text{ \AA}$, $c = 11.5131(4) \text{ \AA}$, $\alpha = 90$, $\beta = 107.398(4)$, $\gamma = 90$, $V = 1860.81(12) \text{ \AA}^3$, $Z = 4$ ($Z' = 1$), $T = 293(2) \text{ K}$, $\mu (\text{MoK}\alpha) = 1.234 \text{ mm}^{-1}$, $D_{\text{calc}} = 1.656 \text{ g/cm}^3$, 20,109 reflections measured ($5.678^\circ \leq 2\Theta \leq 64.758^\circ$), 3093 unique ($R_{\text{int}} = 0.0476$, $R_{\text{sigma}} = 0.0287$) which were used in all calculations, $\rho_{\text{calc}} = 1.656 \text{ g/cm}^3$, $F(000) = 956.0$. The final $R1$ was 0.0280 ($I > 2\sigma(I)$) and $wR2$ was 0.0917 [14]. Fractional atomic coordinates, equivalent isotropic displacement parameters, anisotropic displacement parameters, complete lists of bond lengths and bond angles are summarized in Tables S1–S6 in Supporting Information. The structure is presented at Figure 2 and the selected distances are reported in Tables 1 and 2.

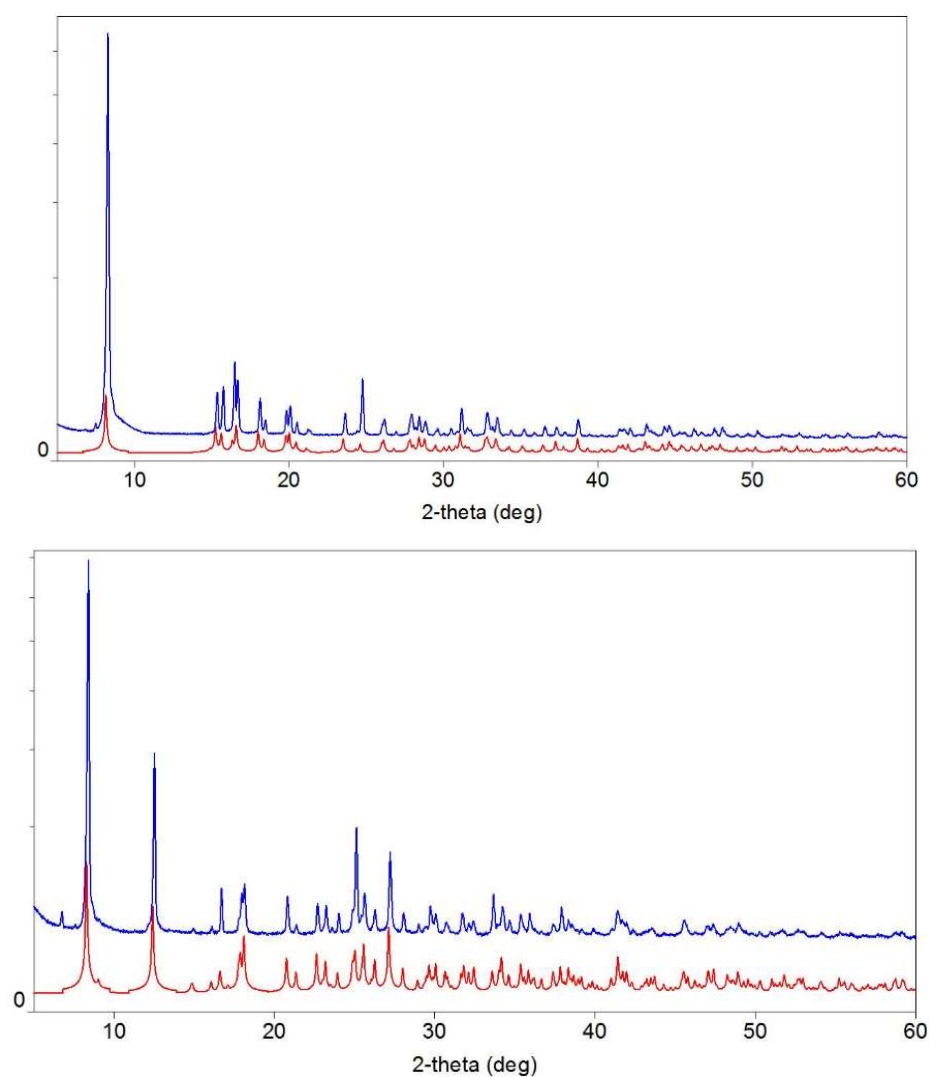


Figure 1. Comparison of powder diffraction pattern for synthesized samples (blue) with those calculated from single crystal X-ray data for disodium (CCDC number 1216797) and dipotassium (CCDC number 1200201) phthalatocuprates (red): **top**—compound I, **bottom**—compound II.

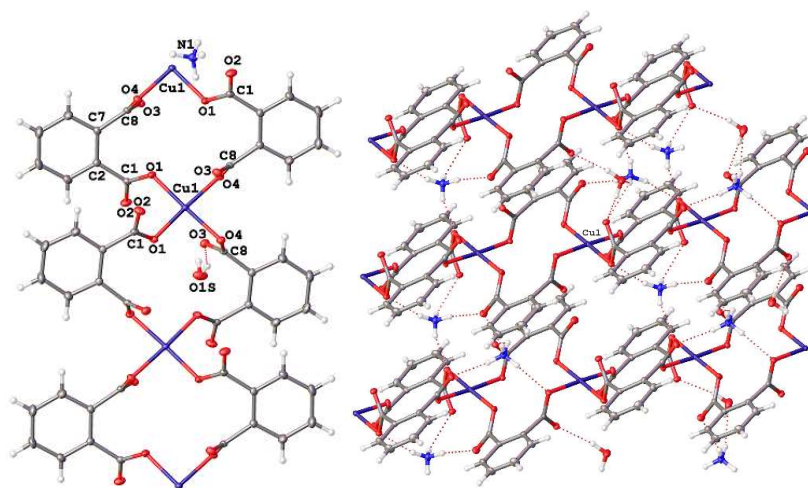


Figure 2. Coordination of *o*-phthalate ligands to copper ion (left) and crystal packing (right) in III. Hydrogen bonds are presented as dotted lines.

Table 1. Bond Lengths for III.

Atom	Atom	Length/Å	Atom	Atom	Length/Å
Cu1	O4 ¹	2.0060(8)	O1	C1	1.2776(14)
Cu1	O4 ²	2.0060(8)	O3	C8	1.2523(13)
Cu1	O1 ³	1.9474(8)	O2	C1	1.2473(14)
Cu1	O1	1.9474(8)	C1	C2	1.5073(15)
O4	Cu1 ¹	2.0060(8)	C8	C7	1.4989(15)
O4	C8	1.2758(13)			

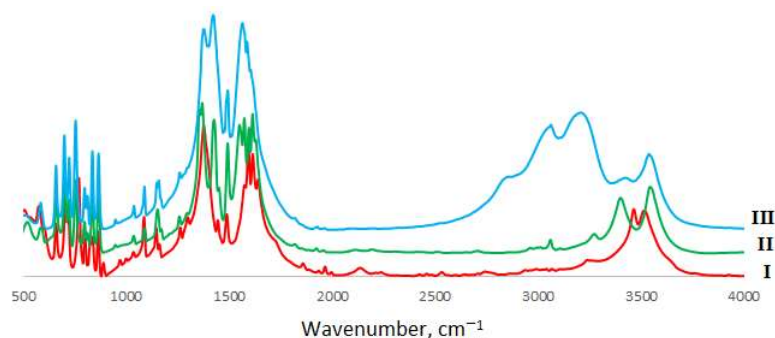
Asymmetric units: ¹ 3/2 - X, 3/2 - Y, 1/2 - Z; ² X, 3/2 - Y, 1/2 + Z; ³ 3/2 - X, Y, 1 - Z.

Table 2. Comparison of selected bonds distances in compounds I–III.

Contact	Distance, Å		
	I	II	III
Cu–O1	1.969(4)	1.999(5)	2.0060(8)
Cu–O4	1.936(3)	1.930(5)	1.9474(8)
C1–O1	1.273(6)	1.263(6)	1.2776(14)
C1–O2	1.237(6)	1.253(6)	1.2473(14)
C8–O3	1.237(6)	1.221(6)	1.2523(13)
C8–O4	1.288(6)	1.296(6)	1.2758(13)

2.4. Vibrational Spectroscopy

Mid-IR spectra have been recorded in the 400–4000 cm⁻¹ spectral region by a Nicolet 8700 (Thermo Scientific, Waltham, MA, USA) spectrometer by means of the ATR technique. Kramers–Kronig correction was applied to eliminate ATR distortions. Far-IR measurements have been performed in the spectral range 65–700 cm⁻¹ at the same equipment. The diffuse reflectance (DRFTS) technique was applied. Raman spectra were recorded by means of SENTERRA (Bruker, Billerica, MA, USA) express Raman spectrometer equipped with Peltier cooled CCD detector (Bruker, Billerica, MA, USA) at 488 nm excitation. For all the spectral measurements 128 scans were performed and averaged, 4 cm⁻¹ spectral resolution was applied. All spectra were measured at an ambient temperature. Baseline correction and deconvolution of spectral contours were made using the GRAMS32 package (Galactic Industries, Salem, NH, USA). The experimental spectra are shown in Figures 3–5, with experimental frequencies summarized in Table S7.

**Figure 3.** Mid-IR spectra of *o*-phthalatocuprates.

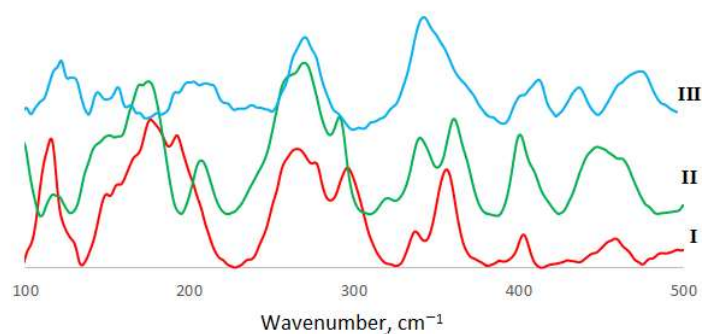


Figure 4. Far-IR spectra of *o*-phthalatocuprates.

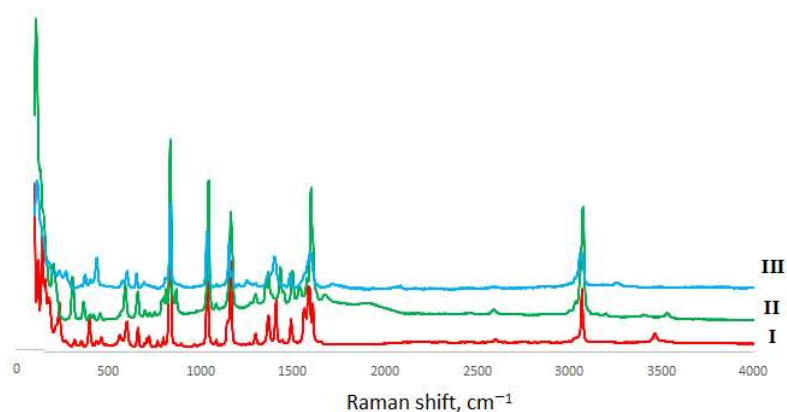


Figure 5. Raman spectra of *o*-phthalatocuprates.

Vibrational bands that appear only in the spectra of compounds **I–III** and are absent in spectra of neat acid were assigned to copper–oxygen stretchings. They were observed as weak to medium intensity bands at 306–307 cm^{-1} (Raman) and 317–319 cm^{-1} (IR). As the geometry of the copper ion coordination sphere is very close to the square planar, we assigned the Raman active frequency to symmetric and another to asymmetric stretching.

To understand in more detail the bonding in alkaline phthalatocuprates, we have undertaken force-field calculations. Though the force constant reflects the slope of the potential energy surface near equilibrium points, for similar molecules, the close relationship in trends for stretching force constants and bond energies is well known. $\text{C}_6\text{H}_4(\text{COOCu})_2$ and $\text{Cu}(\text{OC}(\text{O})\text{C})_4$ moieties were considered to analyze both intraligand bonding and the coordination effect. Wilson’s GF matrix method was used for the calculation of vibrational frequencies using a symmetrized valence force field. The PC-based program package, written in FORTRAN, is developed by J. Mink and L. Mink [15]. Initial force constants were adopted from Colombo et al. [16] and refined to obtain a good coincidence of calculated and experimental data (within 1–2 cm^{-1}). The average experimental frequencies were taken because of the interligand interactions. The experimental and calculated vibrational frequencies of the carboxylate group together with potential energy distribution and refined force constants for this moiety are summarized in Tables 3 and 4 below.

Table 3. Experimental and calculated vibrational frequencies (cm^{-1}) of carboxylate moieties together with potential energy distribution (%) in I–III.

I		II		III		PED	Ass.
Exp.	Calc.	Exp.	Calc.	Exp.	Calc.		
1640	1639	1629	1629	1630	1630	75 $\nu(\text{C}=\text{O})$,	$\nu_{\text{oop}}(\text{C}=\text{O})$
1612	1613	1611	1611	1610	1611	24 $\nu(\text{C}-\text{O})$	$\nu_{\text{ip}}(\text{C}=\text{O})$
1263	1263	1270	1268	1259	1269	63 $\nu(\text{C}-\text{O})$, 21	$\nu_{\text{oop}}(\text{C}-\text{O})$
1265	1263	1258	1260	1252	1260	$\delta(\text{CO}_2)$	$\nu_{\text{ip}}(\text{C}-\text{O})$
660	660	661	660	658	657	68 $\delta(\text{CO}_2)$, 13	$\delta_{\text{oop}}(\text{CO}_2)$
653	654	651	652	653	653	$\nu(\text{C}-\text{O})$	$\delta_{\text{ip}}(\text{CO}_2)$
317	317	319	319	318	317	70 $\nu(\text{CuO})$,	$\nu_{\text{a}}(\text{CuO})$
305	305	307	307	306	306	30 $\delta(\text{CuOC})$	$\nu_{\text{s}}(\text{CuO})$
277	275	272	273	271	269		$\tau_{\text{oop}}(\text{CO})$
267	268	260	261	260	260	90 $\tau(\text{CO})$	$\tau_{\text{ip}}(\text{CO})$

Table 4. Refined force constants for I–III. Stretching force constants are given. 10^2 N m^{-1} , bending— 10^{-18} N m .

Force Constant	I	II	III	Acid [16]
Stretch				
Cu-O	1.465	1.460	1.462	
C-O	6.022	6.071	6.057	5.93
C=O	8.409	8.621	8.616	8.5
C-C	2.503	2.541	2.539	2.6
Stretch-stretch				
Cu-O, Cu-O (trans)	−0.132	−0.167	−0.175	
C-O, Cu-O	0.116	0.125	0.112	
Bending				
CO_2	1.654	1.578	1.589	1.65
CO—torsion	0.266	0.277	0.263	0.21

2.5. Electrochemical Measurements

The electrochemical studies (CorrTest CS300, OhmLiberScience, Saint-Petersburg, Russia) were conducted in a standard three-electrode cell: modified GCE ($d = 3 \text{ mm}$) was used as the working electrode, a platinum mesh as a counter electrode and an Ag/AgCl as reference electrode. Modified GCEs were prepared by sequential drop-casting of $10 \mu\text{L}$ water-based suspension of alkaline di-*o*-phthalatocuprates (1 mg/mL) and $5 \mu\text{L}$ of Nafion solution ($0.02 \text{ wt}\%$); after that, modified electrodes were dried under ambient conditions for further electrochemical experiments. The cyclic voltammetry measurements (CV) were performed within the potential range -0.2 – 0.8 V vs. Ag/AgCl with scan rate of 50 mV/s . The differential pulse voltammograms (DPV) were recorded within the potential range 0 – 0.6 V , with an amplitude of 0.05 V and step potential of 0.004 V . The solutions of analytes (Gl—glucose, DA—dopamine, AP—paracetamol) of different concentrations were added to the corresponding background solutions (0.1 M sodium hydroxide for Gl and 0.1 M PBS for DA and PA).

3. Results and Discussion

3.1. Crystal Structure

The powder diffraction patterns of synthesized I and II compounds (Figure 1) confirmed their phase purity [11]. As ammonium salt (III) was obtained for the first time, single-crystal diffraction study was undertaken. The results have shown that the copper ion in this compound is surrounded by four *o*-phthalate ligands in a nearly square-planar coordination (Figure 2), similar to that in compounds I and II. Copper–oxygen bond lengths in III are equal to $1.9474(8) \text{ \AA}$ and $2.0060(8) \text{ \AA}$ that is rather similar to those in potassium compound II ($1.930(5) \text{ \AA}$ and $1.999(5) \text{ \AA}$ [11]) and a little higher than in sodium salt I ($1.936(3) \text{ \AA}$

and 1.969(4) Å [11]). These bond distances are close to those found in other square-planar copper complexes with *o*-phthalate ligands (1.9336–1.9935 [17,18]). Bond distances in the benzene ring remain the same in all three compounds. As for carboxylate groups, some shortening of C-O bonds is observed in the order of K-NH₄-Na.

The crystal packing in the compounds under study is somehow different. In all three substances, copper ions together with *o*-phthalatoligands form 1D polymeric chains. Water molecules and alkaline cations (or NH₄⁺) are located between adjacent chains and associated 1D chains into 2D layers via hydrogen bonds or electrostatic interactions with phthalate-ions (Figure 2). In (I), the outer-sphere cation (Na⁺) is small enough to be able to be inserted into the hollows of the crossed linear polymeric chains, whereas the increase in ion size prevents this insertion and, as a result, potassium and ammonium ions interpose between adjacent zigzag chains. That results in less distance between the copper ion and non-coordinated oxygen ions from carboxylate groups (2.533 (5) Å and 2.5474 (5) Å in II and III vs. 2.755 (5) Å in I). One can mention that despite the ammonium ion being capable of forming hydrogen bonds with oxygen atoms of carboxylic groups (see Figure S1), which does not effect on the crystal packing in compound III—the effect of ionic size dominates.

3.2. Vibrational Spectroscopy

Vibrational spectroscopy is a powerful tool that enables us to compare bond strengths in chemical compounds without destroying the sample. The assignments of vibrational bands for phthalic acid, the *o*-phthalate ion and the hydrogen *o*-phthalate ion have been undertaken by several researchers: Colombo et al. [16], Arenas et al. [19,20], Martinez et al. [21] and Loring et al. [22]. However, Arenas and Lorig only took into account bands above 1000 cm⁻¹ and Martinez has not analyzed C-H stretchings and carboxylic group vibrations. Therefore, our analysis was based mostly on that performed by Colombo as all vibrational bands of phthalic acid have been taken into account, and the assignment was also supported by quantum chemical calculations and by force field calculations.

That results in values rather similar to those obtained for other benzenedicarboxylic acids (e.g., terephthalic acid and its derivatives [19,20,23–25]). We have only re-assigned an intense band at 832 cm⁻¹ to totally symmetric ring-breathing vibrations instead of OH out-of-plane mode—breathing mode should be the strongest one in Raman spectra. The problem with intensity in the measurements of Colombo et al. [16] can originate from single-crystal (not powdered) Raman measurements. An increase in the number of vibrational modes for alkaline di-*o*-phthalatocuprates(II) is due to the increase in number of *o*-phthalate moieties in the unit cell and interaction between ligands. The complete list of vibrational frequencies and their assignment is given in Table S5.

The comparison of the spectra of *o*-phthalic acid and *o*-phthalatocuprates under study allowed us to assign the modes originating from the carboxylate group (as they are the most affected by coordination to metal ions instead of hydrogen) and metal–ligand modes. Strong to medium intensity bands in the region of 1600–1640 cm⁻¹ were assigned to the C=O stretching mode; lower-frequency modes are more intense in Raman and correspond to in-phase, whereas higher-frequency bands are more intense in IR and corresponds to out-of-phase stretching. The positions of these bands coincide well with those in neat *o*-phthalic acid (1637 and 1640 cm⁻¹). Weak bands at 1250–1270 cm⁻¹ were assigned to C-O stretchings (1263 and 1280 cm⁻¹ in neat acid); a lower frequency compared to acid can result both from the decrease in bond strength and also from the mass difference between hydrogen and copper atoms bonded with the C-O group. The comparison of these data with those for metal ion complexes with terephthalate ligands studied earlier [24,25] shows far less splitting of carboxylate group vibrational frequencies in *o*-phthalate complexes because of non-centrosymmetric position of CO₂ groups.

CO₂ deformations in complexes were found as medium intensity bands at 650–660 cm⁻¹, and C-O twist as a weak to medium intensity band at 265–277 cm⁻¹. As to the bands around 3500 cm⁻¹, they can be attributed to OH stretching modes; the difference in H-bonding in I and II-III can be clearly observed from IR spectra.

As one can see from the obtained results, the force constants obtained are similar to those for phthalic acid. Some increase in C-O stretching force constants reflects a lower polarization effect of copper ions compared to hydrogen. As for copper–oxygen bond strengths, the results are rather similar to those for another complex with oxygen-donor ligands [26]. It should be mentioned that no obvious effect of outer-sphere cations on metal–ligand bond strengths is observed in *o*-phthalatocuprates, in contrast to that found in halide complexes [26,27]. The polymeric structure of complexes and large size of ligands leads to the smoothing of the effect of polarization ability of outer-sphere ions. Intraligand force constants vary to a greater extent, which is probably due to the difference in interaction of outer-sphere cations with the oxygen atoms of carboxylate groups [11].

3.3. Sensor Properties

The monitoring of various analytes in body fluids plays a crucial role in the diagnosis and treatment of many disorders. The changes in glucose level in human blood is closely related to diabetes; in turn, variations in neurotransmitter concentrations (such as DA) are associated with Parkinson disease, Huntington’s chorea, addiction, etc. [28,29]. In this regard, the selective determination of bioanalytes in the presence of the most commonly used drugs worldwide (for example AP) is of great importance not only for clinical practice, but also for biomedical and biochemical research. Electrochemical methods offer a unique combination of expensiveness, flexibility and high performance, and have a great potential in non-enzymatic detection of aforementioned analytes.

The electrocatalytic activities of the synthesized *o*-phthalatodicuprates towards D-glucose oxidation were investigated using CV and CA techniques (Figure 6). Figure 6a,b demonstrate that sensor response toward addition of 3 mM D-glucose is decreased in the order of I > II > III. Therefore, the sample I was chosen for further studies by chronoamperometry, and the typical CA curve recorded during consecutive additions of D-glucose aliquots to 0.1 M NaOH at potentials of 0.55 V presented on Figure 6c. The linear range of dependence of the Faraday current on the D-glucose concentration lies between 1 μ M and 3 mM, wherein sensitivity and the limit of detection (LOD) were equal to 8.95 μ A/mM and 0.26 μ M, respectively. Thereby, sodium salt I exhibits sensor properties comparable with those of another copper-based MOFs known from the literature [30–33]. Table 5 presents the comparison between fabricated glucose sensor and other recently reported ones. Notably, the proposed electrode exhibits comparable characteristics with a wide range of MOF-based sensors including complex composite materials.

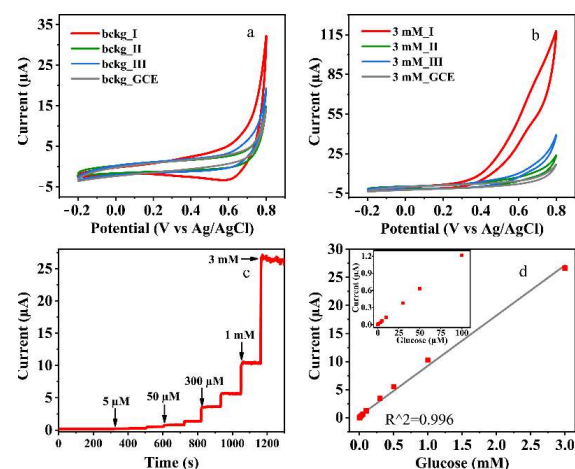
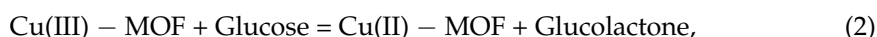


Figure 6. CV of alkaline *o*-phthalatocuprates in (a) background electrolytes and (b) in the presence of 3 mM of D-glucose. (c) Chronoamperogram of I/GCE recorded under potentiostatic conditions 0.55 V and (d) calibration curve for I obtained from CA data (Faraday current vs. [D-glucose]).

Table 5. Electrochemical performance of the sodium *o*-phthalatocuprate/GC electrode and similar materials for enzyme-free glucose sensing.

Electrode Material	Linear Range (μM)	LOD (μM)	Refs.
Cu-MOF/CNHs/GCE	0.25–1200	0.078	30
Multiplayer films of Cu-MOF/MWNTs	0.5–2340	0.4	9
Cu-in-ZIF-8	Up to 700	2.76	31
NiCu-MOF-6	20–4930	15	32
Ni@Cu-MOF	5–2500	1.67	33
Cu-MOF	10–3500	2.4	10
Sodium <i>o</i> -phthalatocuprate/GCE	1–3000	0.26	This work

This difference in sensor properties of the compounds under study cannot be explained by the difference in copper–ligand bonding: both metal–oxygen distances and stretching force constants do not differ so much. According to [9,30], the reaction mechanism involves two steps:



so, the availability of copper ion for nucleophilic attack can play a crucial role. Probably, the major factor affecting the sensor properties of these compounds is more steric hindrance of copper ion in compounds **II** and **III**, where the distance between the copper ion and non-coordinated oxygen ion of phthalate ligands is approximately 10% less compared to that in **I**. As for the difference in properties of potassium and ammonium salts that can result from a different kind of bonding between outer-sphere cations and the ligand—an electrostatic one in **II** and hydrogen bonding in **III**. The formation of hydrogen bond networks should prevent the penetration of the analyte into a complex and its interaction with the metal center that determines the activity according to the established mechanism of glucose oxidation on copper-based electrode materials [34,35].

Furthermore, the determination of AP and neurotransmitter DA in binary mixtures was studied using CV and differential pulse voltammetry techniques (DPV). Figure 7a shows cyclic voltammograms of the **I**/GCE electrode in 0.1 M PBS (pH 7.4); as one can notice, there are two distinct peaks around 0.23 V and 0.49 V corresponding to the oxidation of DA and AP, respectively (Figure S2). DPVs for AP and DA at the sodium di-*o*-phthalatodicuprate-based electrode was obtained by changing the concentration of DA with a fixed concentration of AP (Figure 7b), and vice versa (Figure 7d). The current responses of both substrates increase linearly with their concentrations (Figure 7c,e). The linear regime of AP detection is provided within the range of 3–1500 μM , while there are two linear regions of DA concentration (3–60 μM and 60–500 μM). The calculated limits of detection were equal to 0.95 and 1.17 μM for DA and AP, respectively ($\text{LOD} = 3S/b$. Here, *S* is the standard deviation of ten blank measurements and *b* is the calibration curve slope). The analytical curve equations were found to be:

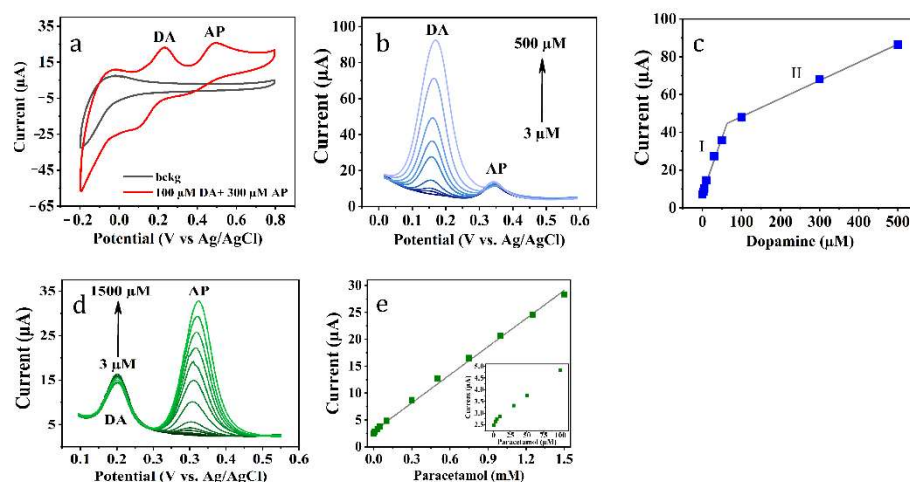


Figure 7. (a) CV of disodium di-*o*-phthalatocuprate-based electrode in background electrolyte and in presence of DA and AP; (b) DPVs of I/GCE recorded in mixture containing 50 μM AP with different concentrations of DA; (d) 20 μM DA with different concentrations of AP; the linear relationship between peak currents and the concentrations of (c) DA and (e) AP.

DA:

$$\text{(I) } I (\mu\text{A}) = 0.589 [\text{DA}] (\mu\text{M}) + 7.669$$

$$\text{(II) } I (\mu\text{A}) = 0.096 [\text{DA}] (\mu\text{M}) + 38.700$$

AP:

$$I (\mu\text{A}) = 0.017 [\text{AP}] (\mu\text{M}) + 2.951$$

4. Conclusions

In summary, the crystal structure of diammonium di-*o*-phthalatocuprate(II) dihydrate was determined for the first time. This structure is nearly identical to that of dipotassium di-*o*-phthalatocuprate(II) dihydrate, which points to the domination of ionic size effect onto possible hydrogen bond formation in alkaline *o*-phthalatocuprates. The vibrational spectroscopic and force field study of disodium, dipotassium and diammonium di-*o*-phthalatocuprates has shown the minor dependence of copper–ligands in intraligand bond strengths on outer-sphere cations in contrast to the complexes with monoatomic ligands that can be explained by rigid polymeric structure of di-*o*-phthalatocuprates under study. Synthesized alkaline di-*o*-phthalatocuprates, especially disodium di-*o*-phthalatocuprate, exhibit electrocatalytic activity towards a range of substrates, among them GI, DA and AP. Better sensor properties of disodium di-*o*-phthalatocuprate are determined by less steric hindrance of copper ions in this compound compared to potassium and ammonium salts that enable the attack of the metal center by incoming ligands. The choosing of proper analytical methods and the optimisation of techniques allow one to fabricate universal electrode material for the selective detection of biosubstances of great importance with decent sensitivity.

Supplementary Materials: The following are available online at <https://www.mdpi.com/article/10.3390/ma14195548/s1>, Table S1: Crystal data and structure refinement for III, Table S2: Fractional Atomic Coordinates ($\times 104$) and Equivalent Isotropic Displacement Parameters ($\text{\AA}^2 \times 103$) for III, Table S3: Anisotropic Displacement Parameters ($\text{\AA}^2 \times 103$) for III, Table S4: Bond Lengths for III, Table S5: Bond Angles for III, Table S6: Hydrogen Atom Coordinates ($\text{\AA} \times 104$) and Isotropic Displacement Parameters ($\text{\AA}^2 \times 103$) for III, Table S7: Vibrational Spectra of Alkaline *o*-Phthalatocuprates and Their Assignment, Figure S1: Ammonium ion interaction with phthalate ions in III, Figure S2: Chemical transformations of (1) GI, (2) DA, and (3) AP during the electrooxidation.

Author Contributions: Conceptualization, M.A.K., E.M.K. and M.Y.S.; Methodology, M.A.K. and E.M.K.; Formal Analysis, A.S.M., and I.I.T.; Investigation, M.V.G., S.V.G., M.A.K., E.M.K. and N.A.B.;

Resources, N.A.B., M.Y.S. and A.S.M.; Data Curation, M.Y.S. and I.I.T., Writing—Original Draft Preparation, M.Y.S.; Writing—Review and Editing, M.A.K., E.M.K. and A.S.M.; Visualization, M.A.K. and A.S.M.; Supervision, A.S.M.; Project Administration, A.S.M.; Funding Acquisition, A.S.M. All authors have read and agreed to the published version of the manuscript.

Funding: The reported study was funded by RFBR, project number 20-33-70025. The electrochemical measurements performed by E.M.K. and I.I.T. were supported by the Fellowship of President of Russia MK-1521.2020.3.

Institutional Review Board Statement: Not applicable.

Informed Consent Statement: Not applicable.

Data Availability Statement: Data is contained within the article or supplementary material.

Acknowledgments: The measurements were performed at the Research Park of Saint-Petersburg State University “Centre for X-ray Diffraction Studies”, “Chemical Analysis and Materials Research Centre”, “Centre for Optical and Laser Materials Research”, “Thermogravimetric and Calorimetric Research Centre”.

Conflicts of Interest: The authors declare no conflict of interest.

References

1. Wang, H.-S. Metal—Organic frameworks for biosensing and bioimaging applications. *Coord. Chem. Rev.* **2017**, *349*, 139–155. [CrossRef]
2. Li, J.; Xia, J.; Zhang, F.; Wang, Z.; Liu, Q. An electrochemical sensor based on copper-based metal-organic frameworks-graphene composites for determination of dihydroxybenzene isomers in water. *Talanta* **2018**, *181*, 80–86. [CrossRef]
3. Anik, Ü.; Timur, S.; Dursun, Z. Metal organic frameworks in electrochemical and optical sensing platforms: A review. *Microchim. Acta* **2019**, *186*, 196. [CrossRef]
4. Wang, X.; Zhang, J.; Wei, Y.; Xing, T.; Cao, T.; Wu, S.; Zhu, F. A copper-based metal-organic framework/graphene nanocomposite for the sensitive and stable electrochemical detection of DNA bases. *Analyst* **2020**, *145*, 1933. [CrossRef] [PubMed]
5. Cheng, D.; Li, X.; Qiu, Y.; Chen, Q.; Zhou, J.; Yang, Y.; Xie, Z.; Liu, P.; Cai, W.; Zhang, C. A simple modified electrode based on MIL-53(Fe) for the highly sensitive detection of hydrogen peroxide and nitrite. *Anal. Methods* **2017**, *9*, 2082–2088. [CrossRef]
6. Brondani, D.; Zapp, E.; Heying, R.S.; Souza, B.; Vieira, I.C. Copper-based Metal-organic Framework Applied in the Development of an Electrochemical Biomimetic Sensor for Catechol Determination. *Electroanalysis* **2017**, *29*, 2810–2817. [CrossRef]
7. Wang, C.; Zhang, H.; Jiang, X.; Zhou, B. Electrochemical Determination of Aflatoxin B1 (AFB1) Using a Copper-Based Metal-Organic Framework (Cu-MOF) and Gold Nanoparticles (AuNPs) with Exonuclease III (Exo III) Assisted Recycling by Differential Pulse Voltammetry (DPV). *Anal. Lett.* **2019**, *52*, 2439–2453. [CrossRef]
8. Song, Y.; Xu, M.; Gong, C.; Shen, Y.; Wang, L.; Xie, L.; Wang, L. Ratiometric electrochemical glucose biosensor based on GOD/AuNPs/Cu-BTC MOFs/macroporous carbon integrated electrode. *Sens. Actuators B* **2018**, *257*, 792–799. [CrossRef]
9. Zheng, W.; Liu, Y.; Yang, P.; Chen, Y.; Tao, J.; Hu, J.; Zhao, P. Carbon nanohorns enhanced electrochemical properties of Cu-based metal organic framework for ultrasensitive serum glucose sensing. *J. Electroanal. Chem.* **2020**, *862*, 114018. [CrossRef]
10. Sun, Y.; Li, Y.; Wang, N.; Xu, Q.; Xu, L.; Lin, M. Copper-based Metal-organic Framework for Non-enzymatic Electrochemical Detection of Glucose. *Electroanalysis* **2018**, *30*, 1011. [CrossRef]
11. Cingi, M.B.; Lanfredi, A.M.M.; Tiripiccio, A.; Camellini, M.T. Influence of the alkaline cation on the structures of polymeric *o*-phthalatocuprate(II). II. The crystal structures of disodium di-*o*-phthalatocuprate(II) dihydrate and dipotassium *catena*-di- μ -*o*-phthalato-cuprate(II) dihydrate. *Acta Cryst.* **1978**, *B34*, 412–416. [CrossRef]
12. Sheldrick, G.M. *SHELXT*—Integrated space-group and crystal-structure determination. *Acta Cryst.* **2015**, *A71*, 3–8. [CrossRef]
13. Dolomanov, O.V.; Bourhis, L.J.; Gildea, R.J.; Howard, J.A.K.; Puschmann, H. *OLEX2*: A complete structure solution, refinement and analysis program. *J. Appl. Cryst.* **2009**, *42*, 339–341. [CrossRef]
14. Cambridge Crystallographic Data Centre, Accession Code 2101455. Available online: www.ccdc.cam.ac.uk/data_request/cif (accessed on 4 August 2021). by e/ailing data_request@ccdc.cam.ac.uk, or by con-tacting The Cambridge Crystallographic Data Centre, 12 Union Road, Cambridge CB2 1EZ, UK; fax: +44 1223 336033.
15. Mink, J.; Mink, L. *Computer Program System for Vibrational Analyses of Polyatomic Molecules. (In Lahey-Fujitsu Fortran WIN32)*; Yumpu, Stockholm University: Stockholm, Sweden, 2004.
16. Colombo, L.; Volovšek, V.; LePostollec, M. Vibrational Analysis and Normal Coordinate Calculations of *o*-Phthalic Acid Molecule. *J. Raman Spectr.* **1984**, *15*, 252–256. [CrossRef]
17. Zhao, H.-X.; Zhuang, G.-L.; Wu, S.-T.; Long, L.-S.; Guo, H.-Y.; Ye, Z.-G.; Huang, R.-B.; Zheng, L.-S. Experimental and theoretical demonstration of ferroelectric anisotropy in a one-dimensional copper(II)-based coordination polymer. *Chem. Comm.* **2009**, 1644–1646. [CrossRef] [PubMed]

18. Wang, X.-L.; Sui, F.-F.; Lin, H.-Y.; Luan, J.; Liu, G.-C. Three Cu (II)/Co (II) Coordination Polymers Constructed From a Flexible Bis-pyridyl-bis-amide and Two Different Polycarboxylates: Assembly, Structure and Properties. *Chin. J. Inorg. Chem.* **2014**, *30*, 2626–2634. [[CrossRef](#)]
19. Arenas, J.F.; Marcos, J.I. Infrared and Raman spectra of phthalate, isophthalate and terephthalate ions. *Spectrochim. Acta* **1979**, *35A*, 355–363. [[CrossRef](#)]
20. Arenas, J.F.; Marcos, J.I. Infrared and Raman spectra of phthalic, isophthalic and terephthalic acids. *Spectrochim. Acta* **1980**, *36A*, 1075–1081. [[CrossRef](#)]
21. De la Blanca, E.S.; Núñez, J.L.; Martínez, P. Vibrational spectra of some o-substituted benzoic acid derivatives. *J. Mol. Struct.* **1986**, *142*, 45. [[CrossRef](#)]
22. Loring, J.S.; Karlsson, M.; Fawcett, W.R.; Gasey, W.H. Infrared spectra of phthalic acid, the hydrogen phthalate ion, and the phthalate ion in aqueous solution. *Spectrochim. Acta* **2001**, *57A*, 1635–1642. [[CrossRef](#)]
23. Tripathi, G.N.R.; Sheng, S.J. Solid-state vibrational spectra and structures of terephthalic acid and the terephthalate ion. *J. Mol. Struct.* **1979**, *57*, 21. [[CrossRef](#)]
24. Geranmayeh, S.; Abbasi, A.; Skripkin, M.Y.; Badiei, A. A novel 2D zinc metal-organic framework: Synthesis, structural characterization and vibrational spectroscopic studies. *Polyhedron* **2012**, *45*, 204. [[CrossRef](#)]
25. Geranmayeh, S.; Abbasi, A.; Zarnani, A.-H.; Skripkin, M.Y. A novel trinuclear zinc metal-organic network: Synthesis, X-ray diffraction structures, spectroscopic and biocompatibility studies. *Polyhedron* **2013**, *61*, 6. [[CrossRef](#)]
26. Stepankova, L.V.; Skripkin, M.Y.; Chernykh, L.V.; Starova, G.L.; Hajba, L.; Mink, J.; Sandstrom, M. Vibrational spectroscopic and force field studies of copper(II) chloride and bromide compounds, and crystal structure of KcuBr. *J. Raman Spectr.* **2008**, *39*, 16. [[CrossRef](#)]
27. Skripkin, M.Y.; Chernykh, L.V.; Pestova, O.N.; Baranaukaite, V.E.; Burkov, K.A.; Zamyatin, I.V.; Stepankova, L.V.; Gusev, I.M.; Gorbunov, A.O.; Bogachev, N.A.; et al. Influence of Interactions in Solutions on the Solid Phase Formation in Ternary Water-Salt Systems. *Russ. J. General Chem.* **2019**, *89*, 1085. [[CrossRef](#)]
28. Klein, M.O.; Battagello, D.S.; Cardoso, A.R.; Hauser, D.N.; Bittencourt, J.C.; Correa, R.G. Dopamine: Functions, Signaling, and Association with Neurological Diseases. *Cell. Mol. Neurobiol.* **2019**, *39*, 31–59. [[CrossRef](#)] [[PubMed](#)]
29. Armstrong, M.J.; Okun, M.S. Diagnosis and Treatment of Parkinson Disease: A Review. *JAMA* **2020**, *323*, 548–560. [[CrossRef](#)]
30. Wu, L.; Lu, Z.; Ye, J. Biosensors and Bioelectronics Enzyme-Free Glucose Sensor Based on Layer-by-Layer Electrodeposition of Multilayer Films of Multi-Walled Carbon Nanotubes and Cu-Based Metal Framework Modified Glassy Carbon Electrode. *Biosens. Bioelectron.* **2019**, *135*, 45–49. [[CrossRef](#)]
31. Shi, L.; Zhu, X.; Liu, T.; Zhao, H.; Lan, M. Sensors and Actuators B: Chemical Encapsulating Cu Nanoparticles into Metal-Organic Frameworks for Nonenzymatic Glucose Sensing. *Sens. Actuators B Chem.* **2016**, *227*, 583–590. [[CrossRef](#)]
32. Pan, W.; Zheng, Z.; Wu, X.; Gao, J.; Liu, Y.; Yuan, Q.; Gan, W. Facile Synthesis of 2D/3D Hierarchical NiCu Bimetallic MOF for Non-Enzymatic Glucose Sensor. *Microchem. J.* **2021**, *170*, 106652. [[CrossRef](#)]
33. Xue, Z.; Jia, L.; Zhu, R.; Du, L.; Zhao, Q. High-Performance Non-Enzymatic Glucose Electrochemical Sensor Constructed by Transition Nickel Modified Ni@Cu-MOF. *J. Electroanal. Chem.* **2020**, *858*, 113783. [[CrossRef](#)]
34. Hwang, D.-W.; Lee, S.; Seo, M.; Chung, T.D. Recent advances in electrochemical non-enzymatic glucose sensors: A review. *Anal. Chim. Acta* **2018**, *1033*, 1–34. [[CrossRef](#)] [[PubMed](#)]
35. Khairullina, E.M.; Panov, M.S.; Andriianov, V.S.; Ratautas, K.; Tumkin, I.I.; Răciukaitis, G. High rate fabrication of copper and copper-gold electrodes by laser-induced selective electroless plating for enzyme-free glucose sensing. *RSC Adv.* **2021**, *11*, 19521–19530. [[CrossRef](#)]